RESEARCH ON DAMPING PERFORMANCE OF ORCHARD FRUIT THREE-STAGE DAMPING TRAILER BASED ON ADAMS
/
基于 ADAMS 的果园果品三级减振拖车减振性能研究

Yifan WANG[1)], Nan AN[1)], Jiaxin LU[1)], Zhihong ZHAO[1)], Xiahui FU[1)], Qingliang CUI[1,2)], Juxia WANG*[1,2)]
[1)]College of Agricultural Engineering, Shanxi Agricultural University, Shanxi Taigu 030801 / China
[2)]Key Technology and Equipment of dry farming agricultural machinery Shanxi Key Laboratory, Shanxi Taigu 030801 / China
Tel: +86-18634418916; E-mail: wangjuxia79@163.com
DOI: https://doi.org/10.35633/inmateh-71-51

Keywords: *orchard transport trailer, D-level pavement, Vibration-damping system, simulation*

ABSTRACT

To enhance the vibration-damping performance of orchard transport trailers and reduce the damage rate during fruit transportation, a D-level simulation pavement was constructed, trailer's vibration-damping system was analyzed and two kinds of three-stage vibration-damping transport trailers were designed and optimized. The vibration mechanical properties of Fuji apples were experimentally evaluated, revealing a positive correlation between damage rate and vibration acceleration. By utilizing vibration acceleration as a vibration-damping parameter, the trailer's vibration-damping performance was simulated by Adams software. The results demonstrated that the three-stage trailer with rubber vibration-damping pads in the horizontal direction exhibited superior vibration-damping effectiveness compared to existing trailers.

摘要

为了提升果园运输拖车的减振性能，降低果品运输的损伤率，本文构建了 D 级仿真路面，对拖车减振系统进行分析，优化设计了两种三级减振果园运输拖车；以富士苹果为研究对象进行了振动力学特性试验，研究获得果品损伤率和振动加速度呈正相关关系；并以振动加速度作为减振参数，运用 Adams 软件对拖车的减振性能进行仿真分析，结果表明水平方向采用橡胶减振垫进行减振的三级减振拖车，相较于现有拖车具备更为优异的减振效果。

INTRODUCTION

In the northwest China, orchards have long sunshine hours, four distinct seasons and a rich variety of fruit trees. Because of the terrain conditions, the transport of orchard fruit mainly rely on human back or the trailer that was hooked up to the tractor. In recent years, the cost of manpower transport has been on the rise due to the continuous decline in the rural labor force; and the vibration-damping performance of current utilization trailer is relatively poor, which resulted in significant damage to a large quantity of fruit during transportation and diminished the economic value of the fruit. However, how to effectively optimize the vibration-damping structure of fruit trailers in orchards is of great significance in reducing fruit damage and improving fruit economic efficiency.

The vibration-damping system of vehicles was generally divided into active vibration-damping *(Teng, 2017; Bai et al., 2018; Yuan, 2022; Ma et al., 2023)* and passive vibration-damping *(Li et al., 2019; Yuan et al., 2020; Yang et al., 2021; Zhao et al., 2019)*, and scholars at home and abroad have carried out some researches on the vibration-damping structure of vehicles and achieved better results. Dong *(Dong, 2022)* constructed a two-stage vibration-damping model of vehicle passive and active suspensions and performed simulation analysis, and found that active vibration-damping had better smoothing performance than passive vibration-damping. Zhou *(Zhou et al., 2021)* executed simulation of vehicle active air suspension and discovered that its vibration-damping performance was better compared to passive air suspension. Chi *(Chi et al., 2017)* designed a hydraulic vibration-damping system, and the simulation results showed that the performance of damping system was improved by 27% compared with the traditional passive damping system in terms of z-direction acceleration and tire deformation.

[1] *Yifan Wang, M.S. Stud. Eng.; Nan An, M.S. Stud. Eng.; Jiaxin Lu, M.S. Stud. Eng.; Zhihong Zhao, M.S. Stud. Eng.; Xiahui Fu, M.S. Stud. Eng.; Qingliang Cui, Prof. Ph.D. Eng.; Juxia Wang, A.P. Ph.D. Eng.*

Zhong *(Zhong, 2020)* designed a three-stage vibration-damped active suspension, and the simulation analysis obtained that the vibration-damping performance of this suspension system was improved by 56.81% and 14.03% compared to the two-stage and one-stage active suspensions, respectively. Shen *(Shen et al., 2016)* designed an ISD suspension structure and indicated that the vibration-damping performance was superior to that of the passive suspension. Suo *(Suo et al., 2021)* proposed a unidirectional coupled oil-air suspension and found that this suspension structure has better vibration-damping performance than the conventional single cylinder oil-air suspension. Qi *(Qi et al., 2023)* designed a tertiary vibration-damping structure after improving the traditional secondary vibration-damping tracked transporter. When driving on C and D road surfaces, the structure improved the vibration-damping effect in the z-direction by 6.4% and 19.6% respectively, and in the x-direction by 18.4% and 17.7% respectively, compared with the secondary vibration-damping structure.

When fruit is harvested in orchards, it is often necessary to attach a trailer due to the limited carrying capacity of the primary vehicle. However, the attached trailer typically employed primary or secondary vibration-damping methods, which exhibited subpar performance in reducing vibrations and consequently resulted in significant fruit damage. In order to minimize fruit damage during transportation in orchards, there is an urgent need to optimize the body's vibration-damping structure of the trailer. In view of this, this paper designed a three-stage vibration-damping trailer for unmanned vehicle hookups in orchards, and determined the relationship between fruit damage rate and vibration acceleration through fruit biomechanical tests; then took the vibration acceleration as the vibration parameter and made a comparison with the existing trailer structure through the simulation analysis of the three-stage vibration-damping trailer. The purpose of the design was to determine that the vibration-damping performance was further optimized and that the three-stage vibration-damping trailer could significantly reduce the damage rate of the fruit and improve the economic benefits of the fruit.

MATERIAL AND METHODS

Model Construction

Orchard pavement model construction

There are five main methods currently used for pavement modeling: harmonic superposition, filtered white noise, inverse Fourier transform and time series modeling *(Shi et al., 2018)*. The method of filtering white noise is a process of fitting the pavement spectrum through a hypothetical transformation when the white noise meets certain conditions. It has the advantages of a complete theoretical basis, few modeling parameters and convenient real-time online simulation, so it is widely used *(Azizi et al., 2022; Qin et al., 2022)*. In this paper, the method of filtered white noise was used to simulate the pavement roughness.

Table 1

Grading standard of pavement roughness

Grade of pavement	Roughness coefficient of pavement $G_q(n_0)$ x 10^{-6} [m^3]		
	upper limit	lower limit	geometric mean
A	32	—	16
B	128	32	64
C	512	128	256
D	2048	512	1024
E	8192	2048	4096
F	32768	8192	16384
G	131072	32768	65536
H	—	131072	262144

Generally, the pavement roughness can be categorized into eight levels (as shown in Table 1). According to the national standard GB/7031-87, the displacement power spectral density of the pavement roughness can be fitted by the power spectral density criterion of single-channel displacement, the formula of power spectral density was defined as:

$$G_q(n) = G_q(n_0)\left(\frac{n}{n_0}\right)^{-w} \quad (1)$$

where:

$G_q(n)$ is displacement power spectral density; $G_q(n_0)$ is roughness coefficient of pavement, [m^3];
n_0 is reference spatial frequency, [n_0=0.1m^{-1}]; W is frequency index, [W=2];
n is spatial frequency of pavement spectrum, [m^{-1}].

Xu *(Xu et al., 2018)* utilized a measuring system to conduct field test measurement and analysis on the pavement roughness of orchards and revealed that the grade of orchard soft and solid dirt pavements in orchards was just between C and D. The fruit trailer designed in this paper was hooked up to an unmanned orchard vehicle for harvesting and transportation of orchard fruits, therefore the Class D pavement was chosen as the simulation pavement model. Based on the filtered white noise method, the Simulink module of MATLAB was used to simulate the pavement roughness simulation, and by changing the speed of the orchard unmanned transport vehicle and the pavement roughness coefficient, the pavement roughness time-domain model of the relevant pavement was obtained, as shown in Fig. 1. The time domain model of filtered white noise pavement roughness is shown as follows *(Yin et al., 2017)*:

$$Z_g(t) = -2\pi n_1 u z_g(t) + 2\pi n_0 \sqrt{G_q(n_0)u}\,\omega(t) \quad (2)$$

where: $Z_g(t)$ is displacement of pavement roughness, [m]; n_1 is cutoff spatial frequency under pavement roughness, [n_1=0.01m^{-1}]; u is vehicle speed, [m/s]; n_0 is reference spatial frequency, [n_0=0.1m^{-1}]; $G_q(n_0)$ is pavement roughness coefficient, [m^3]; $\omega(t)$ is Gaussian white noise, [$\omega(t)$=1].

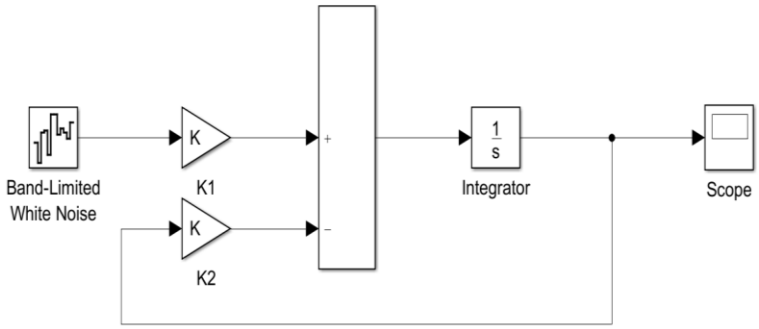

Fig. 1 – Time domain simulation model of pavement roughness

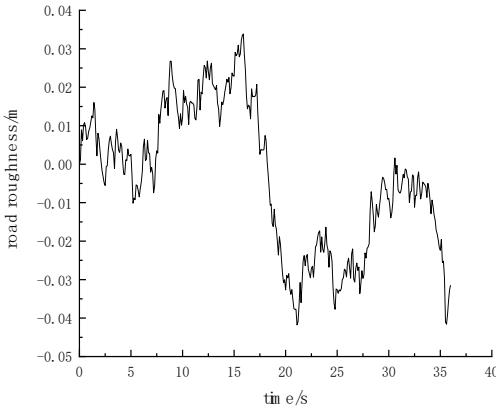

Fig. 2 – Road roughness of Class D pavement

As can be seen in Figure 1, the gain modules were defined as:

$$K1 = 2\pi n_0 \sqrt{G_q(n_0)u}\,\omega(t) \quad (3)$$

$$K2 = 2\pi n_1 u \quad (4)$$

The time-domain model of the pavement roughness of the orchard unmanned transport vehicle was constructed at a vehicle speed of 1 m/s, and the resulting data of pavement roughness were shown in Fig. 2. As can be seen in Fig. 2, the highest value of this pavement roughness data was 0.0339 m and the lowest value was 0.0418 m. These data were used to construct a Class D pavement for subsequent trailer simulation pavement.

Modeling of vibration-damping system

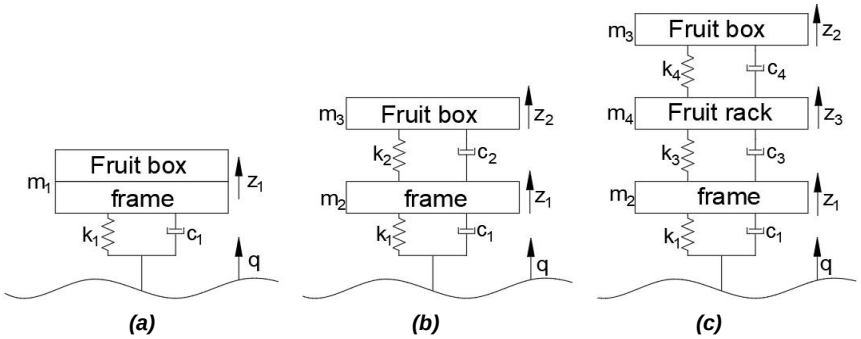

(a) ***(b)*** ***(c)***

Fig. 3 – (a) One-stage vibration-damping system; (b) Two-stage vibration-damping system; (c)Three-stage vibration-damping system

At present, the existing orchard fruit trailers usually use one-stage or two-stage of vibration-damping, and its model simplified diagram of quarter structure is shown in Fig. 3. If the mass and stiffness of the wheel and the deformation of the wheel during travel were neglected, the displacement of the wheel in the z-direction was equal to the pavement roughness. In Fig. 3(a), the equation of the one-stage of the vibration-damping system was defined as:

$$m_1\ddot{Z}_1 + c_1\dot{Z}_1 + k_1Z_1 = c_1\dot{q}_1 + k_1q \tag{5}$$

where: m_1 is mass of transport trailer frames and fruit boxes, [kg]; Z_1 is displacement of the frame by ground excitation, [mm]; k_1 is stiffness of the damping structure between the frame and the axle, [N/mm]; c_1 is damping of damping structures between frame and axle, [N·s/mm]; q is pavement roughness function.

In Fig. 3(b), the equations for the two-stage of vibration-damping system were defined as:

$$\begin{cases} m_3\ddot{z}_2 + c_2\dot{z}_2 + k_2z_2 - c_2\dot{z}_1 - k_2z_1 = 0 \\ m_2\ddot{z}_1 + (c_1 + c_2)\dot{z}_1 + (k_1 + k_2)z_1 - k_2z_2 - c_2\dot{z}_2 = c_1\dot{q} + k_1q \end{cases} \tag{6}$$

where: m_2 is quality of transport trailer frame, [kg]; m_3 is quality of fruit boxes in transportation trailers, [kg]; Z_2 is displacement of a fruit box by ground excitation, [mm]; k_2 is stiffness of the damping structure between the fruit box and the frame, [N/mm]; c_2 is damping of the damping structure between the fruit box and the frame, [N·s/mm].

Because the pavement roughness function changed over time irregularly, it belonged to a non-periodic function. Therefore the pavement roughness function q could be regarded as the action of a series of instantaneous impulses, which might superimpose the system's response to each impulse excitation. Finally the system's response to the pavement roughness excitation was obtained. The system response to impulse excitation could reflect the vibration characteristics of the system.

At moment zero, the response of the system under unit pulse excitation was defined as:

$$h(t) = \frac{1}{m\omega}e^{-\xi\omega_n t}\sin\omega_d t \tag{7}$$

where: $\omega_n = \sqrt{\frac{k}{m}}$, $\xi = \frac{c}{2\sqrt{km}}$, $\omega_d = \omega_n\sqrt{1-\xi^2}$; m is quality of system components, [kg]; k is stiffness of the damping system, [N/mm]; c is damping of damping systems, [N·s/mm].

When the system reached the maximum overshoot M_p that is the 1st arrival at the extreme point, the time set as t_p. The formula of the time t_p was defined as:

$$t_p = \frac{\pi + arctan\frac{\sqrt{1-\xi^2}}{\xi}}{\omega_n\sqrt{1-\xi^2}} \tag{8}$$

The t_p magnitude reflected the speed of the system response and was closely related to the member of the instantaneous acceleration. The time t_p that reached the extreme point was getting longer, the acceleration response of fruit box was getting slower and the instantaneous acceleration was getting smaller. Therefore, in order to improve the vibration-damping performance of the transport trailer, the t_p can be increased by optimizing the structure of the fruit transport trailer. For a vibration-damping system, when the time that the system reached M_p was greater than the time that the pulse reached the peak excitation, a drastically changing signal could be changed into a flat signal.

Optimized design of vibration-damping system

Mathematical model of three-stage vibration-damping system

Existing trailers usually use one-stage or two-stage of vibration-damping, and the trailer vibration that was caused by ground excitation in the transport process was larger, causing serious damage to the fruit. Therefore existing trailers could not meet the requirements of the orchard fruit transport, the vibration-damping structure needed to be optimized for the existing trailer in order to enhance trailer performance and meet the requirements of actual production. Based on the technical requirements of the integration of intelligent unmanned vehicles and agronomy in orchards, a new optimization scheme was proposed for the existing trailer structure. According to the scheme, a three-stage vibration-damping trailer was designed.

The wheels were connected to the axle, the axle was connected to the frame, the frame was connected to the fruit box frame, and corresponding vibration-damping devices were added between the axle and the frame, the frame and the fruit box frame and the fruit box frame and the fruit box respectively.

The trailer adopted wheeled walking and was connected to the unmanned vehicle through the hitch device, and the power and braking of the trailer were provided by the unmanned vehicle, hence the trailer's power system took no account of the design process.

The quarter-structure model of the three-stage vibration-damping system is shown in Fig.3(c). The motion differential equations of the three-stage vibration-damping system model were defined as:

$$\begin{cases} m_3\ddot{z}_2 + c_4\dot{z}_4 + k_4 z_4 - c_4\dot{z}_3 - k_4 z_3 = 0 \\ m_4\ddot{z}_3 + (c_3 + c_4)\dot{z}_3 + (k_3 + k_4)z_3 - c_4\dot{z}_2 - c_3\dot{z}_1 - k_4 z_2 - k_3 z_1 = 0 \\ m_2\ddot{z}_1 + (c_1 + c_3)\dot{z}_1 + (k_1 + k_3)z_1 - k_3 z_3 - c_3\dot{z}_3 = c_1\dot{q} + k_1 q \end{cases} \quad (9)$$

where: m_4 is quality of fruit box frame for transportation trailers, [kg]; Z_3 is displacement of a fruit box frame by ground excitation, [mm]; k_3 is stiffness of the vibration-damping structure between the fruit box frame and the frame, [N/mm]; k_4 is stiffness of vibration-damping structures between fruit boxes and fruit box frame, [N/mm]; c_3 is damping of the damping structure between the fruit box frame and the frame, [N·s/mm]; c_4 is damping of vibration-damping structures between fruit boxes and fruit box frame, [N·s/mm].

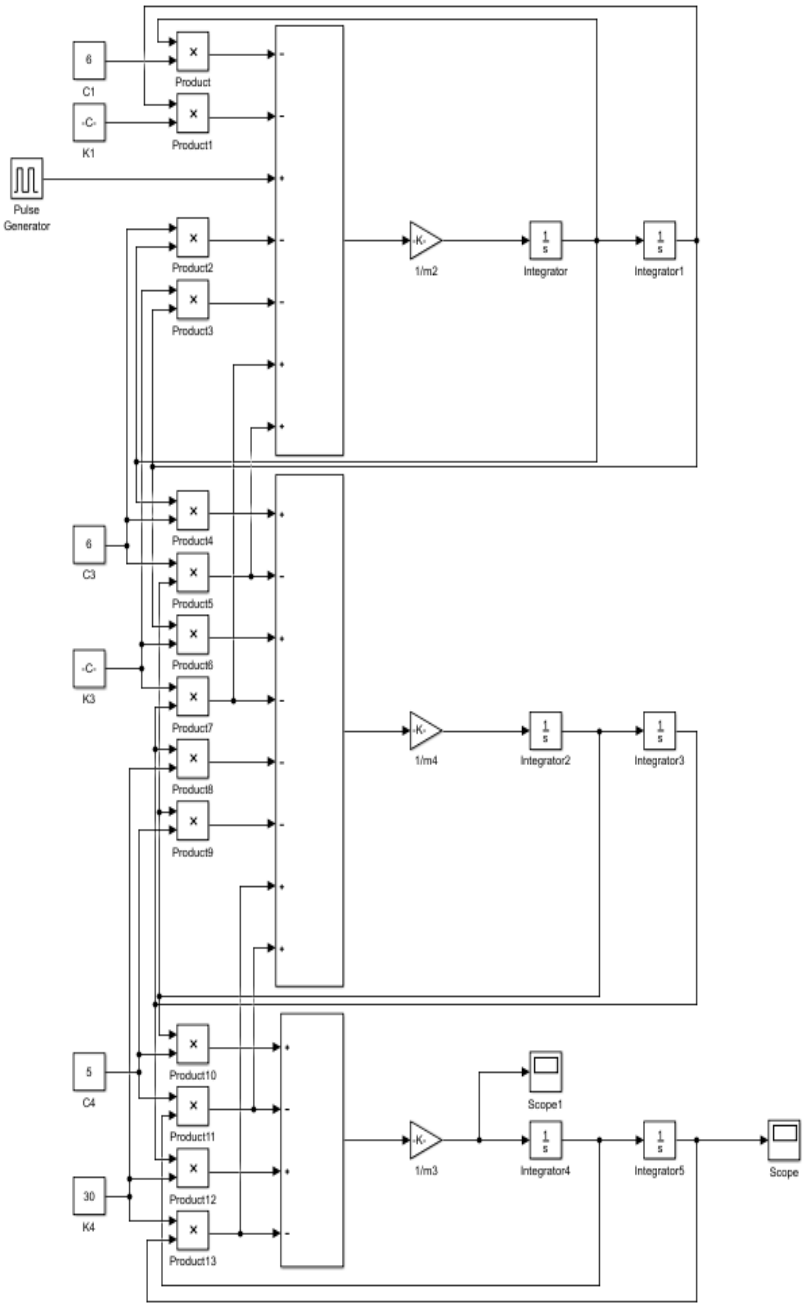

Fig. 4 – Simulink model diagram

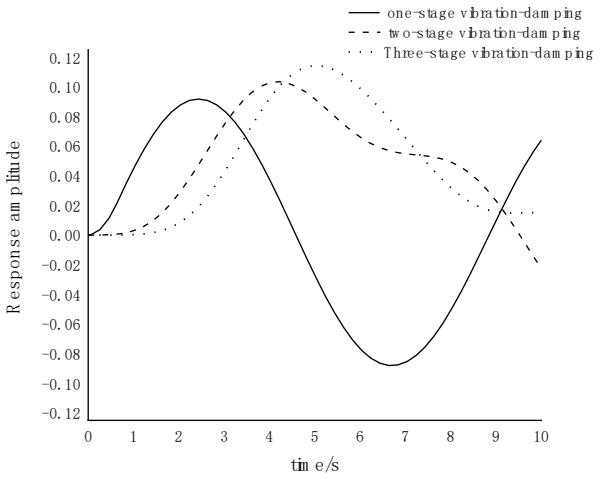

Fig. 5 – Response amplitude diagram of fruit box with different vibration reduction levels

As can be seen from Fig. 5, the t_p of the fruit box of the three-stage vibration-damping transportation trailer was larger than the t_p of the fruit box of the two-stage vibration-damping transportation trailer and was also larger than the t_p of the fruit box of the one-stage vibration-damping transportation trailer. At the same time, the larger the numerical value of t_p was, the slower the change in the amplitude response of the fruit box acceleration was, the smaller the acceleration was, and the smaller the stimulation of the fruits in the fruit box was subjected to. The above analysis expressed that the fruit damage rate that was caused by the three-stage vibration-damping transport trailer was lower than the fruit damage rate that was caused by both the two-stage vibration-damping transport trailer and the first-stage vibration-damping transport trailer under pulse excitation.

Optimized design of three-stage vibration-damping trailer structure

The structure of the one-stage and two-stage vibration-damping trailers for the orchard is schematically shown in Fig. 6. In Fig. 6(a), the one-stage of vibration-damped trailer was vibration-damped by a spring damper, which could reduce vibration-damping for the z-direction excitation that was perpendicular to the ground. Compared with the one-stage of vibration-damped trailer, the two-stage of vibration-damped trailer added rubber vibration-damping pads in the frame to further reduce vibration-damping, as shown in Fig. 6(b). In fact, the rubber vibration-damping pads further reduced the z-direction excitation that was perpendicular to the ground. When the trailer walked on the road, besides vibration excitation from the pavement in the z direction, the trailer also received vibration excitation in the x and y directions, therefore, based on the trailer structure of one-stage and two-stage vibration-damping, two structures of the three-stage vibration-damping trailer were designed (as shown in Fig. 7).

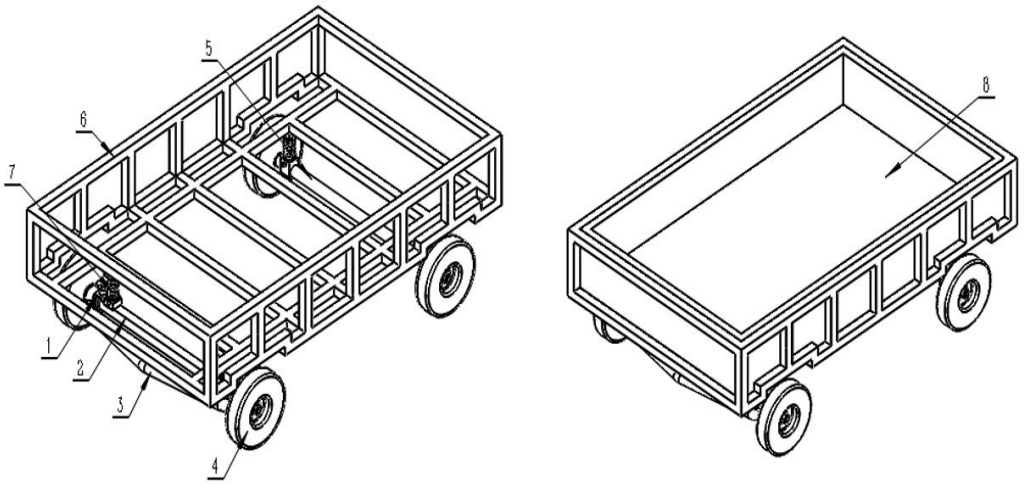

(a) *(b)*

Fig.6 – (a) Structure diagram of one-stage vibration-damping trailer;
(b)Structure diagram of two-stage vibration-damping trailer

1. Steering link 2. Front axle 3. Stabilizer rod 4. Wheels 5. Rear axle 6. Frame 7. Spring shock absorber 8. Rubber vibration pads

In Fig. 7(a), one kind of structure used the spring damper connection not only between the axle and the frame but also between the fruit box frame and the frame, added the rubber vibration-damping pads between the fruit box frame and the frame of the horizontal direction, and added the rubber vibration-damping pads inside the fruit box frame, which not only kept the rubber vibration-damping of the vertical direction unchanged but the vibration excitation of the horizontal direction was also reduced. In Fig. 7(b), another structure replaced the rubber vibration-damping pads between the fruit box frame and the frame with extension springs that had preload.

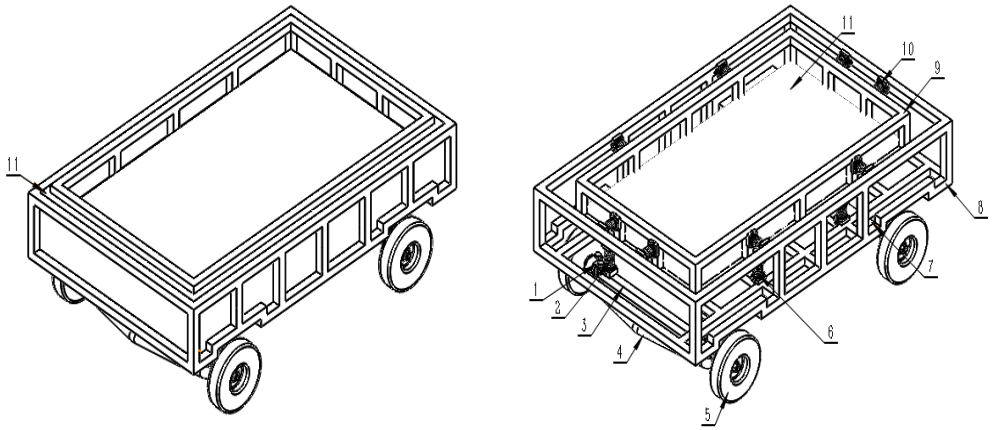

(a) *(b)*

Fig. 7 – Structure diagram of three-stage vibration-damping trailer

1. Steering link; 2. One-stage spring shock absorber; 3. Front axle; 4. Stabilizer rod; 5. Wheels; 6. Two-stage spring shock absorber; 7. Rear axle; 8. Frame; 9. Fruit box frame; 10. Stretch spring; 11. Rubber damping pad

Vibration mechanics property of fruits

Researches have shown that the transportation damage of fruit was one of the important causes of fruit loss, and fruit damage rate in the transportation process could reach 25%~45% *(Lu et al., 2009)*. Therefore, it is necessary to simulate the vibration of the fruit in the transportation process through the shaking table, observe the degree of damage and explore the relationship between the damage rate of the fruit and the vibration acceleration that was generated in the process of vehicle driving.

Test materials and instruments

Fuji apples, which grew in Shanxi Fruit Institute Academy of Agriculture Sciences, were picked in October 2022. In order to minimize the loss of water and other nutrients from the fruits, the picked apples were placed in the laboratory refrigerator at a storage temperature of 3~5℃ to complete the test as soon as possible; the sample fruits were uniformly shaped and sized, no pests and no mechanical damage in the experiment.

In order to simulate the vibration that was generated by the car travel on the pavement, the corresponding vibration excitation of the fruit box were provided by a vibration table (LongData, China); the transverse and longitudinal diameter of apples were measure by electronic vernier calipers with a measurement accuracy of 0.01 mm; the perimeter of apples at the equator was measured by a tape with a measurement accuracy of 1 mm.

Test methods

The 300 apples with undamaged surfaces were selected and weighed, the longitudinal and transverse diameters of the fruits were measured using electronic vernier calipers, the circumference of the fruit equator was measured by a tape and the measurement data were recorded respectively. The 300 fruit samples were divided into 15 groups, and the samples were numbered one by one for each group and loaded into a box measuring 25cm*25cm*25cm, and then the box was numbered.

During the actual transportation, when the pavement was in good condition, the vibration acceleration of the transport car was 0.2~1 g. Therefore vibration acceleration values were set to 0.2 g, 0.25 g, 0.5 g, 0.75 g, 1 g respectively in the simulation test. Considering that the long-distance transportation time of the fruit was generally more than 10 hours, combined with the actual situation, the actual transportation time of the simulation test was set to 15 hours. But in order to ensure the accuracy of the test simulation, based on the research of William and the specific situation of this laboratory, the actual vibration time of the test was reduced to 1/5 of the original, that is to say, the vibration time was 3 h *(Kipp et al., 2000)*.

Table 2

Vibration table debugging data

Sweep frequency [HZ]		20-200	10-500	10-55	10-500	5-80
Acceleration of vibration [g]		1	0.75	0.5	0.25	0.2
Upper limiting frequency (CD000) [HZ]		200	500	55	500	80
Lower frequency [HZ]	CD041	20	10	10	10	5
	CD080	20	10	10	10	5
Upper limit time (CD087) [s]		30	30	30	30	30
Lower limit time (CD088) [s]		30	30	30	30	30
Climbing speed (CD012) [s]		100	36.7	400	36.7	240
Rate of descent (CD013) [s]		100	36.7	400	36.7	240
Total time [s]	CD064	180	180	180	180	180
Amplitude setting [mmp-p]	CD003	58	70	30	60	35
	CD005	15	20	13	18	18

The vibration table adopted the frequency sweep mode, and the relevant debugging data are shown in Table 2. Fifteen boxes of apples were divided into 5 groups and each group carried out a vibration acceleration test (as shown in Fig. 8). At the end of the vibration test, each box of apples was labeled with the start and end time of the test. After the vibrated apples were placed for 24 hours, the damaged apples were selected, and then its damage diameter that was used to do damage grading was measured.

The damage classification method referred to the Agricultural Biomechanics and Agricultural Bio-electromagnetism edited by Sun et al *(Sun et al., 1996)*. Apples that have a damage diameter of less than 19 mm are considered as micro-injury, apples that have a damage diameter of more than 19 mm and less than 25.4 mm are considered as minor injury, apples that have a damage diameter of more than 25.4 mm and less than 31.75 mm are considered as moderate injury, and apples that have a damage diameter of more than 31.75 mm are considered as serious injury *(Sun et al., 1996)*. Therefore the test data were recorded according to the above classification.

Fig. 8 – Process diagram of vibration table test

RESULTS

Analysis of test results

The measurements showed that the mass of the apples ranged from 144 to 326 g, the transverse diameters ranged from 66.39 to 94.52 mm, the longitudinal diameters ranged from 57.78 to 84.48 mm, and the equatorial circumferences ranged from 218.1 to 290.5 mm. After grading the damaged apples in terms of damage diameter, the results obtained are shown in Table 3.

Table 3

Data obtained from grading damaged apples

Accelerated speed [g]	Box number	Number of slight damages	Number of minor damages	Number of moderate damages	Number of severe damages	Total number of damages	Damage rate [%]	Average damage rate [%]
0.2	1	3	2	0	1	6	30	23.33
	2	4	0	0	0	4	20	
	3	3	1	0	0	4	20	
0.25	4	4	1	0	0	5	25	26.67
	5	5	0	0	0	5	25	
	6	5	1	0	0	6	30	
0.5	7	6	0	0	0	6	30	31.67
	8	5	1	0	0	6	30	
	9	4	3	0	0	7	35	
0.75	10	6	2	0	0	8	40	36.67
	11	4	3	0	1	8	40	
	12	4	2	0	0	6	30	
1	13	8	4	0	0	12	60	50
	14	5	3	0	0	8	40	
	15	8	2	0	0	10	50	

(a) slight damage *(b) minor damages* *(c) severe damages*

Fig. 9 – Damage diagram of apples with different damage levels

As can be seen from Table 3, for the same vibration time, the higher the vibration acceleration, the higher the damage rate of apples. The damage grade of apples were mostly micro-injury, light injury, and very few were serious injury, which was consistent with the actual transportation condition. The damage situation of apples with different damage levels is shown in Fig. 9.

The unitary linear regression analysis of vibration acceleration and fruit damage rate was carried out by SAS software. The results showed that the determination coefficient of the regression model amounted to 0.9522, which indicated that the regression model had very high fitting accuracy and could be used as a response prediction. The regression equation is as follows:

$$y = 0.174 + 0.30126x \quad (10)$$

The relationship between the measured apple damage rate and the unitary linear regression curve is shown in Fig. 10. From Fig. 10, the vibration acceleration that was generated during vehicle traveling and the fruit damage rate presented positive linear correlation. Therefore the subsequent simulation tests could use vibration acceleration as a vibration-damping parameter to evaluate the vibration-damping performance of the designed three-stage vibration-damping trailer.

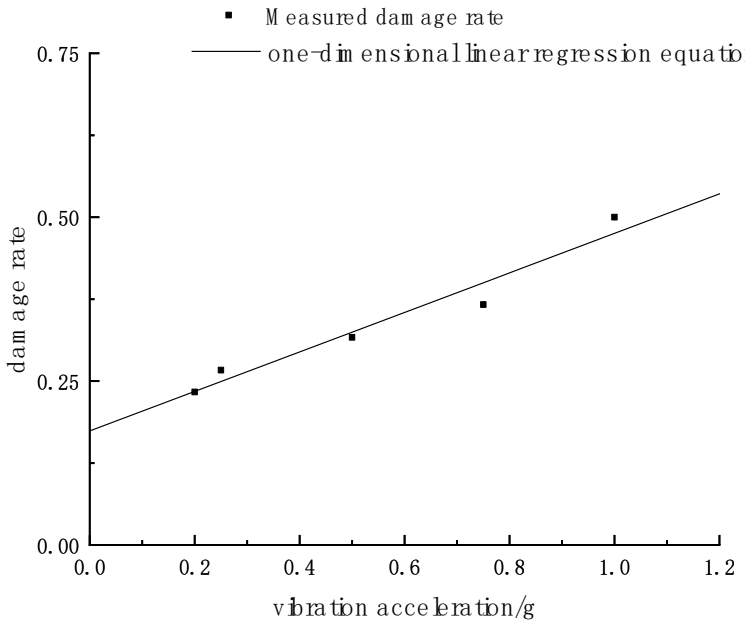

Fig. 10 – Relationship between measured fruit damage rate and unitary linear regression curve

Dynamics Simulation Analysis

Dynamic simulation analysis of the trailer structure was carried out using Adams software to test the vibration acceleration generated by the one-stage, two-stage and three-stage vibration-damped trailer when driving on Class D road surface, respectively. The relevant parameters of the trailer are shown in Table 4.

Table 4

Values of trailer related parameters

Title	Symbolic representation	Numerical value	Unit
Frame quality	m_4	110	kg
Fruit box stand quality	m_2	70	kg
Fruit box quality	m_3	200	kg
First level vibration-dampening stiffness	k_1	42.06	N/mm
First level vibration-dampening damping	c_1	1.5	N s/mm
Second level vibration-dampening stiffness	k_3	34.11	N/mm
Second level vibration-dampening damping	c_3	1.5	N s/mm
Third level vibration-dampening stiffness	k_4	7.5	N/mm
Third level vibration-dampening damping	c_4	0.3	N s/mm
Tension spring stiffness	k_5	34.11	N/mm
Car speed	v	1	m/s

z-direction simulation results and analysis

The one-stage vibration-damped trailer, the two-stage vibration-damped trailer, and both structures' three-stage vibration-damped trailer each drove for 36 seconds on a D-class pavement at a speed of 1 m/s, and the acceleration response values of the fruit box were used as the simulation results.

The acceleration response of the fruit box in the z-direction is shown in Fig. 11.

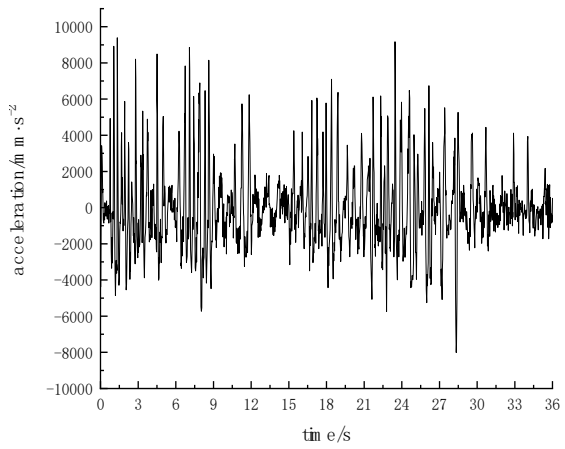

(a) acceleration response graph of one-stage vibration-dampening trailer in the z-direction

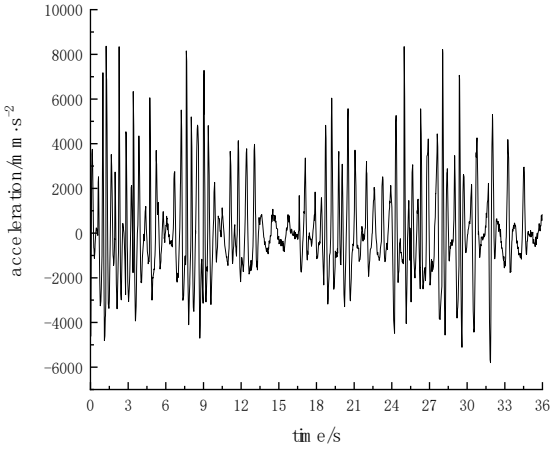

(b) acceleration response graph of two-stage vibration-dampening trailer in the z-direction

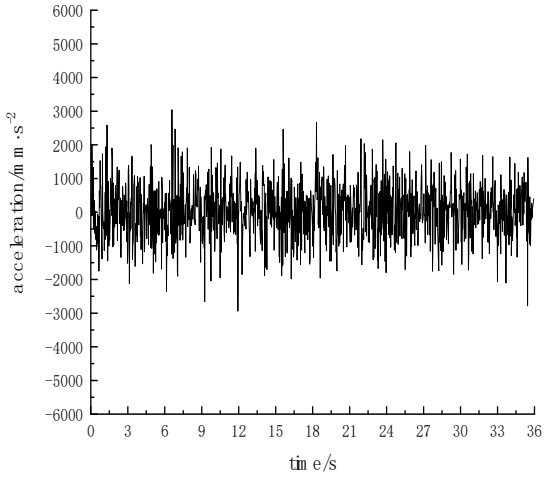

(c) acceleration response graph of three-stage vibration-dampening trailer Fig. 7(a) in the z-direction

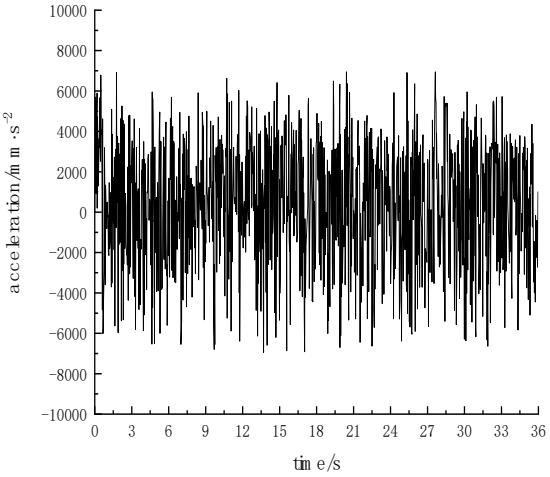

(d) acceleration response graph of three-stage vibration-dampening trailer Fig. 7(b) in the z-direction

Fig. 11 – Acceleration response diagram in the z direction of the fruit box

Based on Class D pavement, the z-direction acceleration optimization effect of the four structures of vibration-damped trailers is compared as shown in Fig.12.

From Fig.12, when the vibration-damped trailer was driving on the pavement of Class D, the acceleration mean square deviation of the two-stage vibration-damped trailer in the z-direction was optimized by 7.4% compared with that of the one-stage vibration-damped trailer and the acceleration peak value was optimized by 10.9%.

For the three-stage vibration-damped trailer rubber vibration-damping pads were utilized in the horizontal direction, the mean squared error of acceleration in the z-direction was optimized by 16.8% compared to the one-stage vibration-damped trailer and 10.2% compared to the two-stage vibration-damped trailer, and the peak acceleration was optimized by 20.7% compared to the one-stage vibration-damped trailer and 11.0% compared to the two-stage vibration-damped trailer.

For the three-stage vibration-damped trailer with tension spring in the horizontal direction, the mean squared error of acceleration in the z-direction was optimized by 23.0% compared to the one-stage vibration-damped trailer and 16.9% compared to the two-stage vibration-damped trailer, and the peak acceleration was optimized by 25.9% compared to the one-stage vibration-damped trailer and 16.8% compared to the two-stage vibration-damped trailer. The above analysis showed that the two kinds of three-stage vibration-damped trailers had better vibration-damping performance than the traditional one-stage and two-stage vibration-damped trailers in the z-direction.

The three-stage vibration-damped trailer that used tension spring for vibration-damping in the horizontal direction had better vibration-damping performance in the z-direction than the three-stage vibration-damped trailer that used rubber vibration-damping pads for vibration-damping in the horizontal direction.

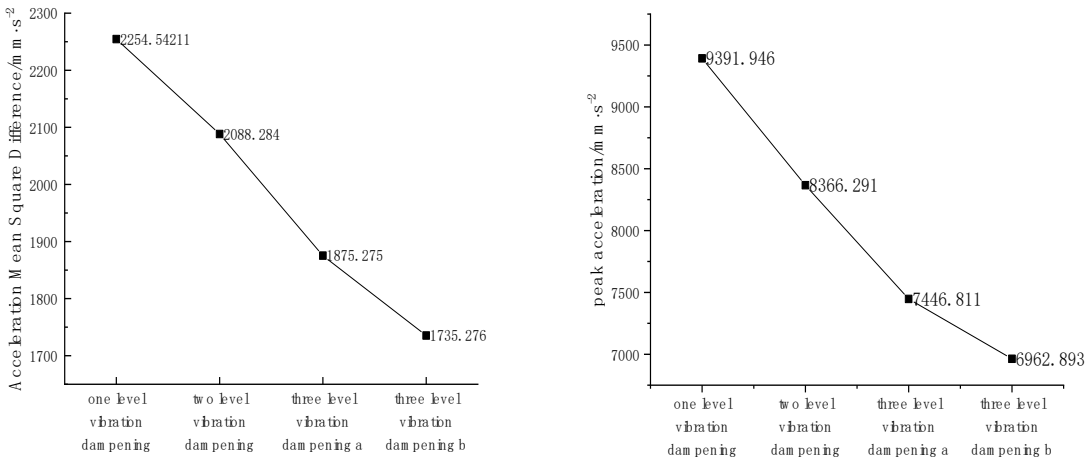

(a) z-direction acceleration mean square deviation *(b) Peak z-direction acceleration*

Fig. 12 – Comparison diagram of Z-direction optimization effect

x- and y-direction simulation results and analysis

When the trailer was in the process of driving, the fruit box would not only be excited by the vibration from the ground in the z-direction, but also by the vibration in the x-direction and y-direction. Therefore the vibration effect of the x-direction and y-direction needed to be simulated and analyzed. The acceleration response of the fruit box in the x-direction and y-direction are shown in Fig. 13 and Fig. 14, respectively.

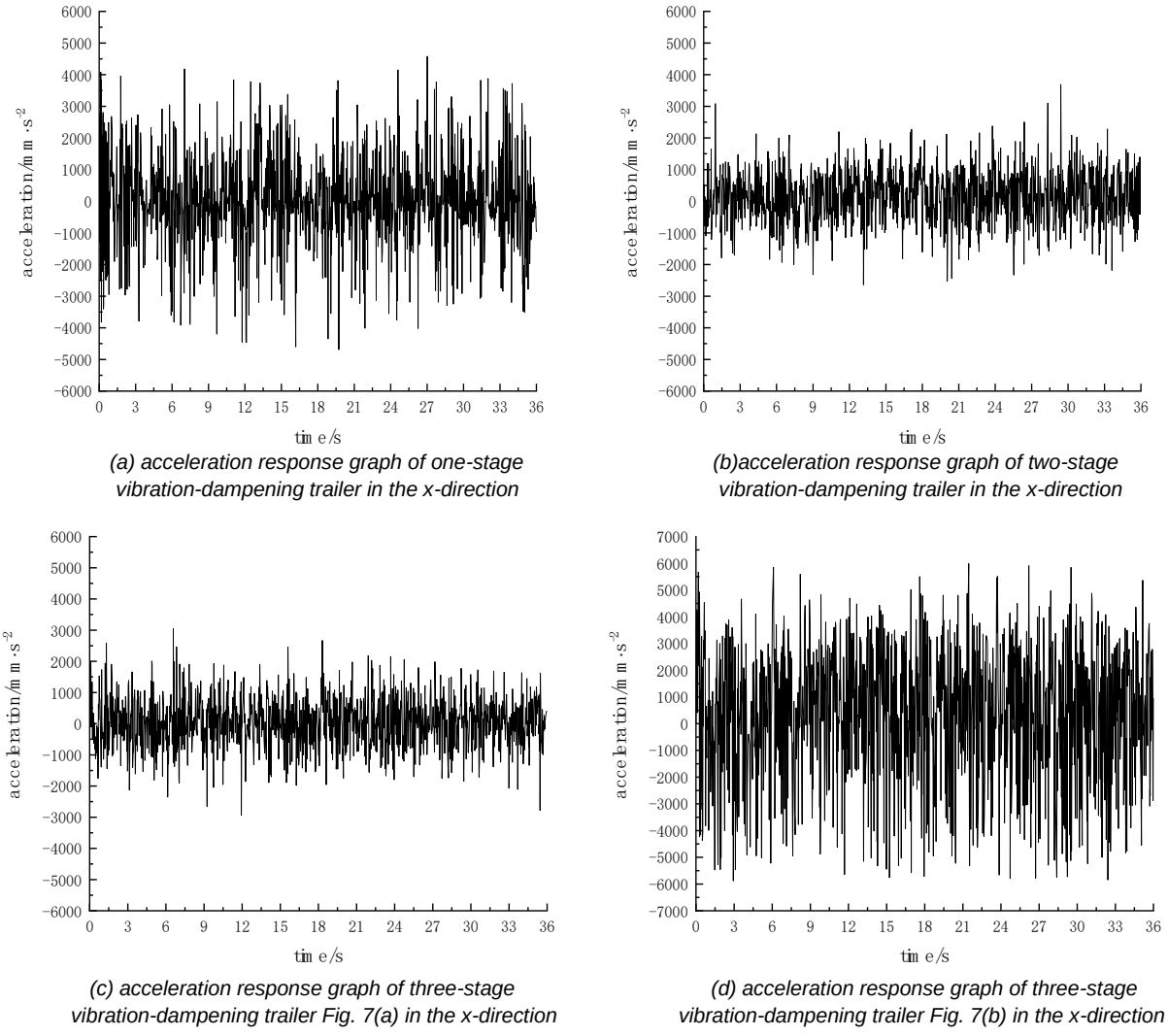

(a) acceleration response graph of one-stage vibration-dampening trailer in the x-direction

(b)acceleration response graph of two-stage vibration-dampening trailer in the x-direction

(c) acceleration response graph of three-stage vibration-dampening trailer Fig. 7(a) in the x-direction

(d) acceleration response graph of three-stage vibration-dampening trailer Fig. 7(b) in the x-direction

Fig. 13 – Acceleration response diagram in the x direction of the fruit box

When the vibration-absorbing trailers of four structures were driving on the D-class road surface, the optimization effects of X-direction and Y-direction acceleration are compared in Fig.15 and Fig.16 respectively. From Fig. 15, the acceleration mean square deviation of the two-stage vibration-damped trailer in the x-direction was optimized by 41.2% and the peak acceleration is optimized by 19.4% compared with that of the one-stage vibration-damped trailer. For the three-stage vibration-damped trailer utilized rubber vibration-damping pads in the horizontal direction, its mean squared error of acceleration in the x-direction was optimized by 43.3% compared to the one-stage vibration-damped trailer and 3.5% compared to the two-stage vibration-damped trailer, and its peak acceleration was optimized by 33.5% compared to the one-stage vibration-damped trailer and 17.5% compared to the two-stage vibration-damped trailer. For the three-stage vibration-damped trailer with tension springs in the horizontal direction, the mean square deviation of acceleration in the x-direction increased by 73.7% compared with the one-stage vibration-damped trailer and 195.4% compared with the two-stage vibration-damped trailer, and the peak acceleration increased by 30.7% compared with the one-stage vibration-damped trailer and 62.2% compared with the two-stage vibration-damped trailer.

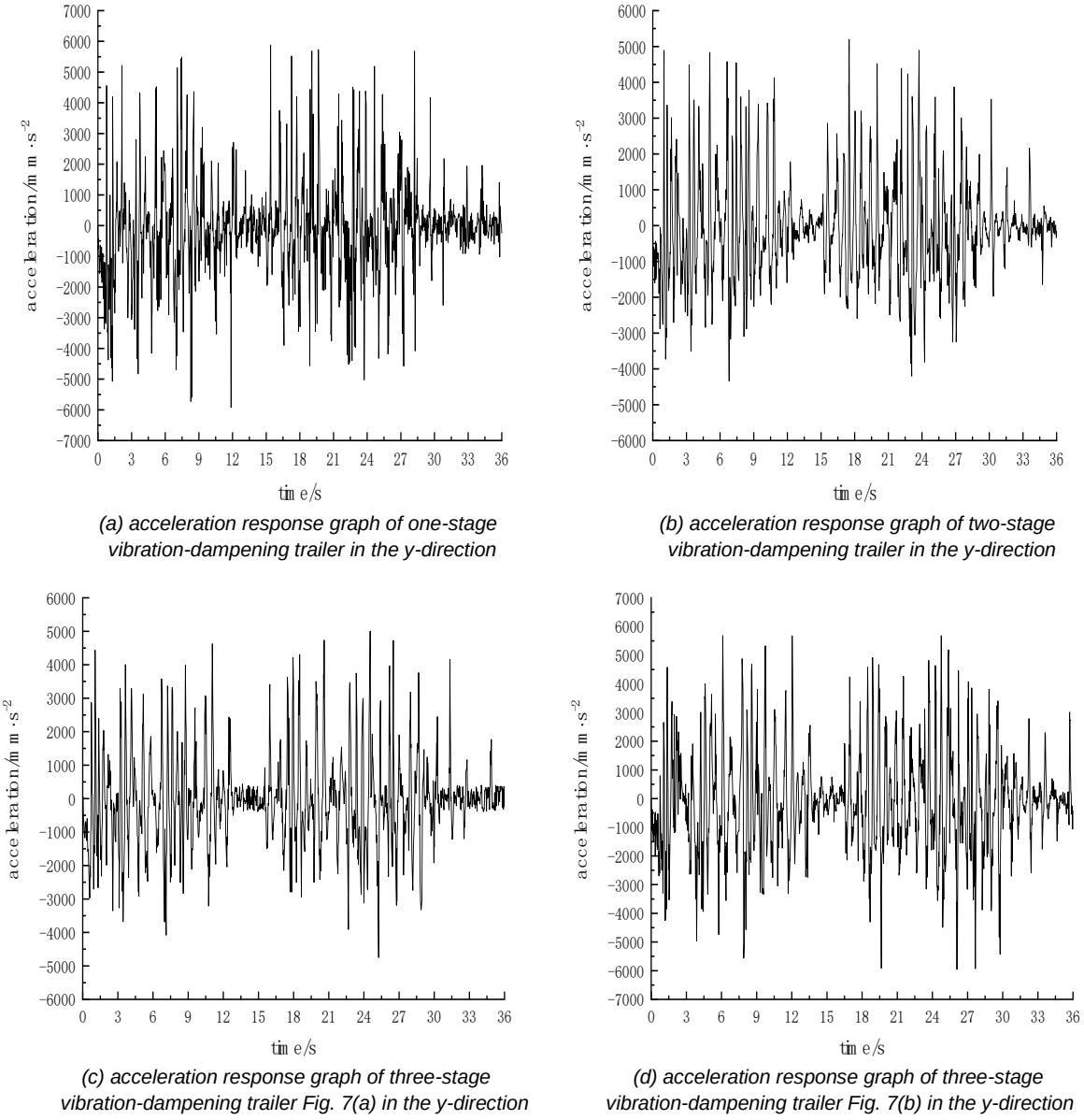

(a) acceleration response graph of one-stage vibration-dampening trailer in the y-direction

(b) acceleration response graph of two-stage vibration-dampening trailer in the y-direction

(c) acceleration response graph of three-stage vibration-dampening trailer Fig. 7(a) in the y-direction

(d) acceleration response graph of three-stage vibration-dampening trailer Fig. 7(b) in the y-direction

Fig. 14 – Acceleration response diagram in the y direction of the fruit box

As can be seen from Fig. 16, the acceleration mean squared error of the two-stage vibration-damped trailer in the y-direction was optimized by 11.9% compared with the one-stage vibration-damped trailer, and the peak acceleration was optimized by 11.7%. For the three-stage vibration-damped trailer with rubber vibration-damping pads in the horizontal direction, the mean squared error of acceleration in the y-direction

was optimized by 13.4% compared to the one-stage vibration-damped trailer, 1.7% compared to the two-stage vibration-damped trailer, and the peak of acceleration optimized by 14.9% compared to the one-stage vibration-damped trailer and 3.6% compared to the two-stage vibration-damped trailer. Whereas, for the three-stage vibration-damped trailer with tensile springs in the horizontal direction, the mean squared error of acceleration in the y-direction was optimized by 14.9% compared to the one-stage vibration-damped trailer and 30.4% compared with the two-stage vibration-damped trailer, and the peak acceleration by 12.6% over the one-stage vibration-damped trailer and 27.5% over the two-stage vibration-damped trailer.

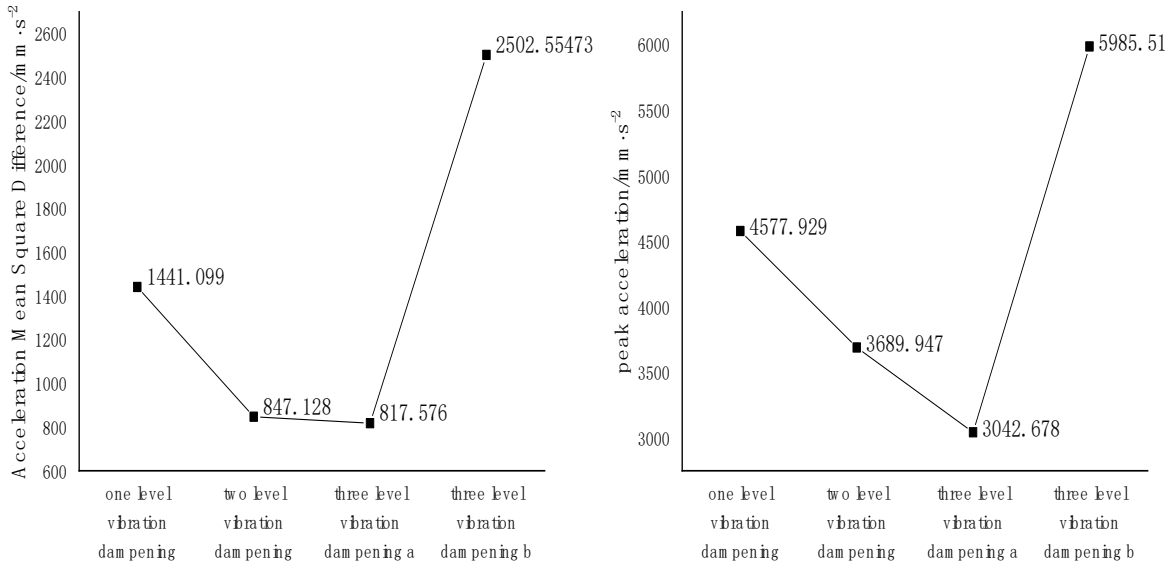

(a) x-direction acceleration mean square deviation *(b) Peak x-direction acceleration*

Fig. 15 – Comparison diagram of x-direction optimization effect

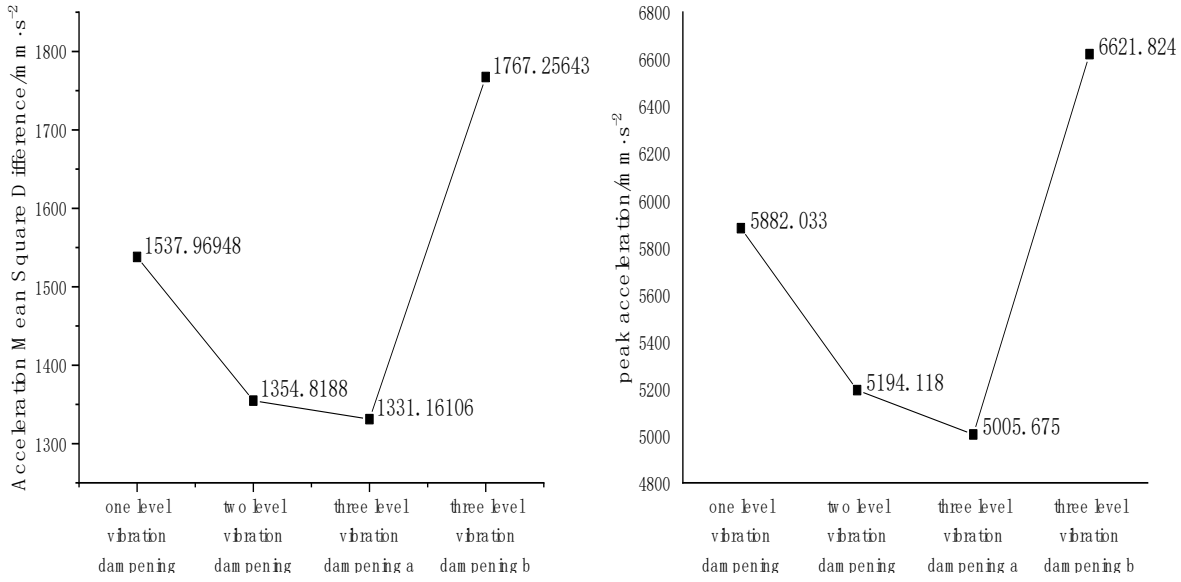

(a) y-direction acceleration mean square deviation *(b) Peak y-direction acceleration*

Fig. 16 – Comparison diagram of y-direction optimization effect

The above analysis showed that for the damping performance of the two designed three-stage vibration-damping trailers in the x and y directions, the three-stage vibration-damping trailer with rubber vibration-damping pads in the horizontal direction was better than the conventional one-stage vibration-damping trailer and two-stage vibration-damping trailer, while the three-stage damping trailer with tension springs in the horizontal direction had a worse vibration-damping performance than the conventional one-stage vibration-damping trailer and two-stage vibration-damping trailer in the x and y directions. Meanwhile, in the x and y directions, the three-stage vibration-damping trailer with rubber vibration-damping pads in the horizontal direction was better than the three-stage vibration-damping trailer with extension springs in the horizontal direction.

CONCLUSIONS

(1) Based on the pavement model of the orchard, the dynamics analysis of the vibration-damping system of the orchard transportation trailer was carried out, and two kinds of three-stage vibration-damping transportation trailers were designed; the results of the vibration mechanics test by the fruits showed that the damage rate of the fruits and the vibration acceleration were positively correlated, which provided a reference basis for the simulation test to evaluate the vibration-damping performance of the designed trailer.

(2) Taking the vibration acceleration as the vibration-damping parameter, the acceleration response diagram of the vibration-damping trailer that was driving at 1 m/s on the D-class road was generated by Adams simulation, and the results showed that compared with the one-stage and two-stage vibration-damping trailer, the optimization rates of the three stage vibration-damping trailer that had rubber vibration-damping pads of the horizontal direction were 16.8% and 10.2% respectively, and the optimization rates of the three stage vibration-damping trailer that had extension springs of the horizontal direction were 23.0% and 16.9% respectively.

(3) When driving on Class D pavement, for the three-stage transport trailer using a rubber vibration-damping pad in the horizontal direction, its vibration-damping optimization rates were 43.3% compared with the one-stage vibration-damping trailer in the x direction and 13.4% in the y direction, and its vibration-damping optimization rates are 3.5% compared with the two-stage vibration-damping trailer in the x direction and 1.7% in the y direction. For the three-stage vibration-damped trailer with tension springs in the horizontal direction, the vibration acceleration in the x- and y-directions was respectively increased by 73.7% and 14.9% compared to the one-stage vibration-damped trailer and by 195.4% and 30.4% compared with the two-stage vibration-damped trailer, and thus its vibration-damping performance in the x- and y-directions was worse than that of the existing trailer.

In short, the vibration-damping effect of the three-stage vibration-damping trailer that used rubber vibration-damping pads in the horizontal direction was the best, which could better achieve the purpose of improving the vibration-damping performance of a mountain orchard transportation trailer.

ACKNOWLEDGEMENT

The authors were funded for this project by the Key R&D Program of Shanxi Province (No.202102020101012), the National Natural Science Foundation of China (No.11802167) and science and the Applied Basic Research Project of Shanxi Province (No.201801D221297).

REFERENCES

[1] Azizi, A., (2018). Computer-Based Analysis of the Stochastic Stability of Mechanical Structures Driven by White and Colored Noise. *Sustainability* (10).

[2] Bai, R., Guo, D., (2018). Sliding-Mode Control of the Active Suspension System with the Dynamics of a Hydraulic Actuator. *Complexity*.

[3] Chi, Y., Ren, J., Wang, Y., Ji, X.Y., & Li, J.Q., (2017). Design and Simulation of Wheeled Tractor Hydraulic Active Suspension System (轮式拖拉机液压减振系统的设计与仿真分析). *Journal of Agricultural Mechanization Research* (09), 46-50, Haerbing/China.

[4] Dong, M.F., (2022). Modeling and Simulation of Different Vehicle Suspension Systems (车辆不同悬架系统的建模仿真分析). *Automobile Applied Technology* (21), 123-126, Xi'an/China.

[5] GB/T 7031－2005, Mechanical vibration—Road surface profiles—Reporting of measured data (机械振动 道路路面谱测量数据报告).

[6] Kipp, W.I., (2000). Vibration testing equivalence. *In ISTA Con,* Vol. 2006, No. 26, pp. 1-13.

[7] Li, X.P., Li, F.J., Cao, Z., & Yang, L.X., (2019). Vibration Performance of Two-Stage Vehicle Suspension with Inerters (含惯容器的两级汽车悬架振动性能). *Journal of Northeastern University (Natural Science)* (10), 1448-1453, Shenyang/China.

[8] Lu, L.X., Huang, X.F., & Hua, Y., (2009). Effect of packaging methods on vibration bruising of pear fruits by simulated transport tests (基于模拟运输条件的梨果实包装振动损伤研究). *Transactions of the Chinese Society of Agricultural Engineering* (06), 110-114, Beijing/China.

[9] Ma, T.G., Zeng, J.S., Feng, P.J., Yang, Y.Y., & Zhang, W.H., (2023). Research on hybrid damping semi-active vibration reduction control of secondary suspension of superconducting electric maglev train (超导电动磁悬浮列车次级悬挂混合阻尼半主动减振控制研究). *Journal of Mechanical Engineering* (10), 236-249, Beijing/China.

[10] Qi, D.Z., Ruan, X.S., Wu, Y.Z., Sun, Q., & Gao, W.Z., (2023). Optimal Design of Vibration Damping System for Transport Vehicles between Rows in Mountain Orchards (山地果园行间运输车减振系统优化设计). *Journal of Agricultural Mechanization Research* (10), 237-242, Haerbing/China.

[11] Qin, Y., Langari, R., Wang, Z., Xiang, C., & Dong, M. (2017). Road profile estimation for semi-active suspension using an adaptive Kalman filter and an adaptive super-twisting observer. *In 2017 American Control Conference* (ACC) pp. 973-978. IEEE.

[12] Shen, Y.J., Chen, L., Yang, X.F., & Yang, J., (2016). Improved design of dynamic vibration absorber by using the inerter and its application in vehicle suspension. *Journal of Sound and Vibration*.

[13] Shi, X.H., Jiang, X., Zhao, J., & Zhai, J.X., (2018). Research on vehicle-road coupling dynamic load on uneven pavement (不平路面车路耦合动载研究). *China Sciencepaper* (04), 408-413, Beijing/China.

[14] Sun, Y.Y., Yu, D.Y., (1996). Agri-biomechanics and agri-bioelectromagnetics (农业生物力学及农业生物电磁学). *China Agriculture Press,* Beijing/China.

[15] Suo, X.F., Jiao, S.J., Wang, G.F., Liu, S.M., & Zhang, Z.Y., (2021). Research on the Vibration Damping Performance of a Novel Single-Side Coupling Hydro-Pneumatic Suspension. *Tehnički vjesnik* (5).

[16] Teng, F.H., (2017). Study on optimization of suspension and Vibration reduction performance of tracked armored vehicle (履带式装甲车悬挂优化及减振性能研究). MD Dissertation, Zhongbei University, Shanxi/China.

[17] Xu, Z.F., Xue, X.Y., & Cui, L.F., (2017). Measurement and Analysis of Farmland Surface Roughness (农田地面不平度测量与分析). *Journal of Agricultural Mechanization Research* (01), 171-176, Haerbing/China.

[18] Yang, M., Zhang, J., & Luo, X.J., (2021). Research on New Types of Suspension Vibration Reduction Systems (SVRSs) with Geometric Nonlinear Damping. *Mathematical Problems in Engineering*.

[19] Yin, J., Chen, X.B., Wu, L.X., & Liu, Y.L., (2017). Simulation Method of Road Excitation in Time Domain Using Filtered White Noise and Dynamic Analysis of Suspension (滤波白噪声路面时域模拟方法与悬架性能仿真). *Journal of Tongji University (Natural Science)* (03), 398-407, Shanghai/China.

[20] Yuan, D.F., (2022). *Research on Semi-active control strategy of vehicle-mounted vibration isolation platform adopting continuously adjustable damper (基于连续可调半主动减振器的车载隔振平台控制策略研究).* MD Dissertation, Jilin University, Jilin/China.

[21] Yuan, J.Q., Zhou, Y.Q., Fan, J., & Lu, Z.X., (2020). Research on vibration characteristics of tractor driving on the farmland (农田行驶工况下拖拉机振动特性研究). *Journal of Chinese Agricultural Mechanization* (02), 127-134, Nanjing/China.

[22] Zhao, Y.Q., Xu, H., Deng, Y.J., & Wang, Q.W., (2019). Multi-objective optimization for ride comfort of hydro-pneumatic suspension vehicles with mechanical elastic wheel. Proceedings of the Institution of Mechanical Engineers, Part D: *Journal of Automobile Engineering* (11).

[23] Zhong, J.G., (2020). *Research on Modeling and Control of Three-stage Vibration Reduction Active Suspension (三级减振式主动悬架建模与控制研究).* MD Dissertation, Zhejiang Sci-Tech University, Zhejiang/China.

[24] Zhou, Y.Q., Li, L.Q., Sun, F.J., Wang, Y., Sun, M., & Li, H., (2021). Simulation Analysis of Active Air Suspension of Heavy-Duty Vehicle Based on Fuzzy PID Control (基于模糊 PID 控制重型汽车主动空气悬架仿真分析). *Automobile Parts* (05), 25-28, Guangzhou/China.